Finite Element Analysis and Simulation of Lag Screw Insertion by Robotic Arm for Basicervical Hip Fractures

Filippos Vlontakis[1], Pantelis Nikolakopoulos[1], Panagiotis Koustoumpardis[2], Antonios Kouzelis[3], Antonis Sakellarios[4]

[1] Machine Design Laboratory, Mechanical and Aeronautical Engineering. University of Patras, 26500 Patras, Greece.
[2] Robotics Group, Department of Mechanical Engineering and Aeronautics, University of Patras, 26334 Patras, Greece
[3] Department of Orthopedics, General University Hospital of Patras, 26504 Patras, Greece
pnikolakop@upatras.gr

Abstract

Hip fractures are severe conditions, associated with reduced quality of life and high mortality rates. Basicervical femoral neck fractures, a relatively rare type of hip fractures, are associated with high internal failure fixation rates, due to the inherent rotational instability of the fracture pattern. It has been shown that, during lag screw insertion for internal fixation, the femoral head may rotate with relation to the femoral neck, leading to greater risk malunion or nonunion and finally, of implant failure post-surgery. This work focuses on the finite element modelling of an empirical surgical technique of lag screw insertion developed by the orthopedic department at the university hospital of Patras, with the goal of limiting the relative rotation between femoral head and neck. Then, a simulation of a robotic arm performing the insertion of the lag screw is developed, to demonstrate potential feasibility of such a system. Using Quantitative CT (QCT) scans of the proximal femur, a 3D model of the femur with inhomogeneous material properties was generated. The Finite Element model (FEM) simulated the insertion procedure of the lag screw according to the surgical technique. The equivalent environmental stiffness of the system was estimated from the results of the model and used to simulate the behavior of a robotic manipulator during insertion. The maximum relative displacement suggests that the proposed surgical technique could be effective in limiting relative sliding. The errors observed during the robotic arm simulation suggest that the use of such a system could be feasible. The methodology employed highlights the usefulness of physics-based simulations in pre-operative planning.

Keywords: Basicervical hip fracture, Orthopedic biomechanics, Finite Element Analysis, Robotic-assisted surgery, Simulation

1 Introduction

The rapid ageing of the population, with the subsequent rise in age-related illnesses and subsequent strain on national health systems, are two of the most pressing issues of modern societies. Osteoporosis and osteoporosis-related fractures are common amongst the elderly and are associated with severe costs and implications for the patients. Of those, proximal femur or hip fractures are considered very severe, as they have been associated with high mortality risks and reduction of quality of life [1]. According to an estimation from the International Osteoporosis Foundation, it is expected that 6% of males and 18% of females will require hospitalization due to hip fractures [2], while projections estimate that hip fracture-related surgeries will rise to 4.5 million per year by 2050 [3]. The costs of hospitalization are also significant, with one study finding that each hip fracture surgery has an average cost of 12.000$ for the US national healthcare system [4].

Basicervical femoral neck fractures account for 1.8-7.6% of all femoral neck fractures [5] and are considered a relatively rare subtype. Due to the fracture pattern, which promotes the development of shear stresses along the fracture line and at the implant, basicervical fractures are inherently unstable [6]. Due to this instability, basicervical femoral neck fractures are associated with high rates of fixation failure and reoperation [7]. Currently, no clear guidelines exist for the treatment of such fractures [8]. Current clinical data suggests that both arthroplasty and internal fixation methods are used at about the same rate [9]. In the case of internal fixation, no clinical evidence favors cephalomedullary or extramedullary implants [6]. It has been reported that during lag screw insertion, the femoral head-neck fragment may rotate in relation to the femoral diaphysis, therefore increasing instability of the fracture after fixation and contributing to an increased risk of aseptic necrosis and non-union [10].

Finite element analysis (FEA) has been widely used in the biomechanical modelling of the proximal femur, to estimate fracture risk, assess and compare implant performance, and more recently, as a tool for pre-operative planning.

Personalized modelling has been employed in the quest for developing more accurate fracture risk prediction markers, that integrate physics-based knowledge of the hip, for patients at high risk of fracture [11–13]. Finite element has enabled detailed stress analysis without the variability inherent in physical testing. Sophisticated three-dimensional models have been widely developed to investigate the biomechanical performance of various implants under different loading conditions, providing valuable comparative data [14–16]. The methodology typically involves constructing 3D models of both the femur and implant systems, followed by the application of simulated physiological loading conditions that mimic standing, walking, or other activities [14, 17] Such numerical models can offer an attractive alternative to expensive experimental techniques, especially in the case of comparative analyses of novel implant systems [15, 18]. Recently, efforts have been made to incorporate FEA workflows to generate clinically relevant data for pre-operative planning in the case of proximal femur fractures [19] and other proximal femur conditions [20], due to the ability of detailed analysis of the in-vivo responses of the system [20], and the possibility of integration with computer assisted planning systems, to effectively help surgeons to make accurate and clinically relevant preoperative planning [21].

Robotic-assisted surgery (RAS) has been a novel technological advancement, employed in orthopedic surgical procedure as a solution that improves precision and reproducibility mainly in joint reconstruction, joint replacement and spinal surgical procedures [22]. Robotic systems such as MAKO and ROSA for total knee and hip replacement, have enabled the use of preoperative 3D planning using CT scans, allowing surgeons to optimize implant positioning and balance soft tissues intraoperatively [23, 24]. As far as spinal surgeries are concerned, a 2023 meta-analysis of lumber fusion cases reported a 98.7% screw accuracy rate with robotics, compared to 92.1% in freehand techniques, while reducing fluoroscopy time by 38% [25].

While RAS systems, whether autonomous or semi-autonomous, have been greatly developed over the past decade and short-term outcomes have been promising, long-term data (>10 years) on implant survivorship in robotic cases remains limited. Current consensus guidelines recommend selective use in complex primary cases and revisions rather than routine implementation [23, 24]. Recently, efforts to expand the application of RAS have been undertaken in trauma orthopedic surgery, for example for the precise fracture reduction in periarticular fractures, using haptic-guided systems [26].

The scope of this work is dual: (i) a Finite Element Model (FEM) of the insertion procedure of a lag screw in the case of a basicervical fracture will be developed using clinical data and (ii) a simulation of the insertion procedure executed by a robotic arm using results from the FEM will be implemented. The goal is to illustrate the potential beneficial uses of physics-based simulations in pre-operative planning, in terms of predicting the behavior of the fracture during surgery, assisting in better implant placement and fracture reduction for this challenging surgical procedure and additionally, the potential for the development of a semi-automated surgical procedure for the treatment of basicervical fractures.

2 Methods

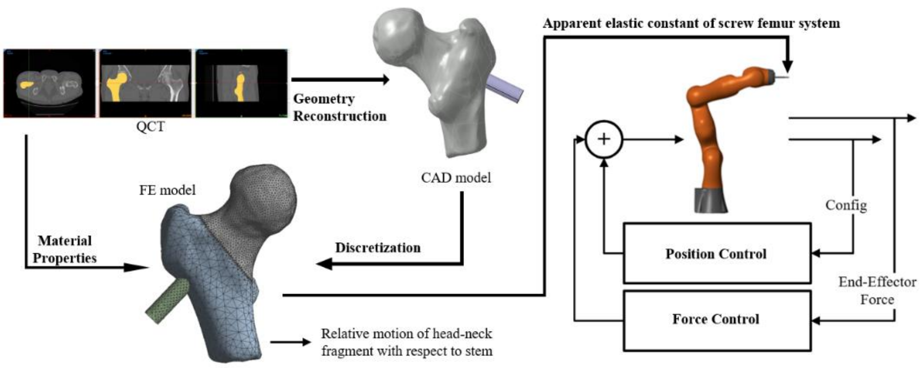

Fig. 1. Methodology Outline.

The outline of the proposed methodology is presented in Fig. 1. First a Quantitative Computed Tomography (QCT) scan is segmented and a model of the proximal femur with inhomogeneous material properties is generated. Then, using results from the model, a control scheme for the robotic arm is designed to automate the insertion procedure.

2.1 Finite Element Model of Lag Screw Insertion

Geometry

The geometry of the lag screw was modelled using the Strycker's Gamma3 Lag Screw in combination with the Gamma3 Intertrochanteric Nail. Only the Lag Screw was modelled, as the nail has no effect on the sliding behavior of the head-neck fragment studied for the scope of this study.

The geometry of the proximal femur was obtained employing a typical medical imaging workflow. One random QCT scan was obtained from a cohort of osteoporotic women, in DICOM format, from a previous study. The area of the femur was then segmented using the 3D Slicer software [27], through semi-automated methods. From the segmented scan, a surface mesh was generated, which was used to create a solid CAD model of the proximal femur. Employing the guidelines set by [28], the anterior-posterior and inferior-superior lines of the proximal femur were defined to assist in the positioning of the lag screw. The fracture was introduced through a virtual fracture line, indicative of the typical geometry of a basicervical hip fracture following the clinical advice.

Positioning of the lag screw in the final assembly was done according to the optimal position for post-operative results, as shown in the work of Konya et al. For the scope of this work, the lag screw is considered in a position partially inserted in the femoral head-neck fragment but not yet having reached its ultimate position in the femoral head. Drilling of the bone is considered to have preceded lag screw insertion and threads to have already been cut. Fig. 2 presents the geometries of the femur and screw geometry.

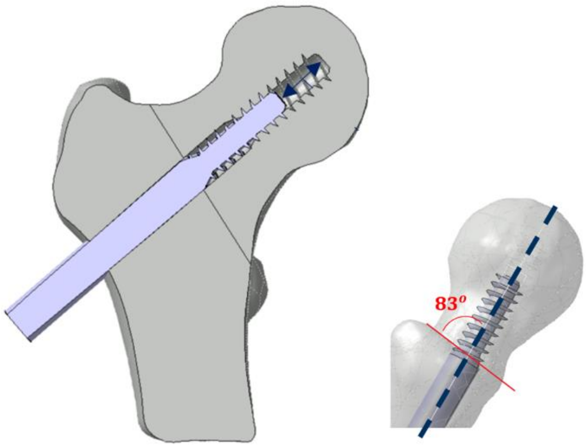

Fig. 2. Anteroposterior (left) and top-down (right) view of the proximal femur geometry.

Finite Element Analysis

The finalized assembly was then meshed using 10-node tetrahedral elements, which are well equipped for handling the complex geometries of both the femoral bone and the treads of the lag screw. The final meshed femur geometry has 280674 elements while the lag screw 75990 elements.

The material assigned to the lag screw was Ti6Al4V. To model the inhomogeneous material properties of the bone, the radiodensity field of the QCT scan, calculated at each voxel, expressed in Hounsfield Units, HU, was converted to radiographic density, ρ_{QCT}, which was then calibrated to ash density, ρ_{ash}, according to the relationships reported in [29]. Ash density was converted to local Young's modulus, E, at each voxel through the empirical relationship reported in [30] (eq. 1-3). The voxel mesh was then mapped to the unstructured mesh of the model to obtain the material properties of each element using the open-source software BoneMat [28].

$$\rho_{QCT} = -0.00393573 + 0.000791701 * HU \quad [{}^{g}/_{cm^3}], \tag{1}$$

$$\rho_{ash} = 0.0079 + 0.877 * \rho_{QCT} \left[{}^{g}/_{cm^3}\right], \tag{2}$$

$$E = 14664 * {\rho_{ash}}^{1.49} \, [MPa], \tag{3}$$

An important aspect of the model is contact modelling. Two different types of contact are considered. The bone-implant interface contact, present at the interface of the lag screw and the head-neck fragment, is modelled by both a static and a dynamic friction coefficient, as determined experimentally in the work of Grant et al. [31], and the transition from the former to the latter is described by the exponential decay law, which is an expression for the friction coefficient, μ, as a function of the relative sliding speed between the bone and implant surfaces, v:

$$\mu(v) = 0.38 + (0.41 - 0.38)e^{-10v}. \tag{4}$$

The bone-bone interface between the two bone fragments is modelled only by a static friction coefficient, as it is expected that the relative motion between the fragments will be minimal. The interface between the lag screw and the intertrochanteric region is modelled as frictionless, to reduce computational cost, as the effect of friction at that interface are assumed to have no significant effect on the relative motion of the head-neck fragment.

The boundary conditions are defined in accordance with the empirical surgical technique proposed by the orthopedic department at the University Hospital. The surgical technique employed by the surgeons is a two-step process. After the lag screw has initially been inserted and some threads are in contact with the neck-head fragment, the compression screw of the implant system is tightened, with the goal of pretension development along the main axis of the screw. Due to this pretension force, a frictional contact force is developed at the bone fragments interface. Then, the lag screw is rotated and inserted into the head-neck fragment, up until the compression screw requires re-tightening. To simulate the surgical technique, the boundary conditions are broken into two steps. Initially, a tractive force is developed at the body of the screw, to mimic the effect of the compression screw. Then, the lag screw is rotated for a total of 70 degrees. Only this initial phase of rotation is modelled, as it is assumed that the critical phase of the operation is before and immediately after initial sliding at the bone-implant interface has occurred.

2.2 Simulation of Robotic Arm

The simulation of the semi-automated insertion of the lag screw in the proximal femur was implement using a Multiphysics model of a Kuka IIWA, 7 degree of freedom (DoF), robotic arm. This redundant manipulator is converted to non-redundant by considering the revolute joint at the base of the manipulator to be welded. For simplification of the simulation, it was also assumed that the main lag screw axis was aligned with the x-axis of the world frame. Therefore, the problem of the application of a force and rotation along the main axis of the screw, is instead treated as a problem of applying a force along and a rotation around the x-axis of the world frame.

For the control of the manipulator, a hybrid force-position control scheme was implemented, as shown in **Fig. 1**. The position controller of the hybrid scheme is designed to control the rotation around the x-axis, that is, one DoF is controlled through position. The other five DoFs are controlled by the force controller. Initially, during the tractive force development phase, the rotation reference input is zero, while the x-axis force is being developed as discussed in the FE simulation. After the tractive force development phase, the force input remains constant and the screw is rotated, initially accelerating and after a point reaching a constant rotational insertion speed. The input forces and moments in the y, z axes of the world frame are zero, to minimize the unnecessary stresses on the femur.

One important aspect of the force controller of the control scheme is the estimation of the stiffness k of the environment, or, more specifically, in this case, the stiffness of the screw-proximal femur system as shown by eq. 5, where $\underline{f_c}$ is the force control signal, $\underline{f}$ is the actual force at the end-effector, $\underline{\tilde{f}} = \underline{f_c} - \underline{f}$ is the force error and $\boldsymbol{k}_P{}^f, \boldsymbol{k}_I{}^f, \boldsymbol{k}_D{}^f$ are the proportional, integral and differential controller gains respectively. This estimation cannot be made simply from the elastic modulus of the materials involved, as the thread interface is complex, and the apparent stiffness of the system depends primarily on the behavior of the treaded interface. To obtain an estimation of the apparent stiffness of the environment, the slope of the curve of the change in tractive force at the head of the screw applied in the FEM, ΔF, against the displacement of the head of the screw, Δz, as evaluated by the model, as calculated (eq. 6).

$$\underline{f_c}(t) = \underline{f} + \frac{1}{k}\left(\underline{\ddot{f}} + \boldsymbol{k}_D{}^f \underline{\dot{\tilde{f}}} + \boldsymbol{k}_P{}^f \underline{\tilde{f}} + \boldsymbol{k}_I{}^f \int \underline{\tilde{f}}\right), \tag{5}$$

$$k = \frac{\Delta F}{\Delta z}\ [N/m]. \tag{6}$$

3 Results and Discussion

The finite element (FE) analysis of the lag screw insertion procedure revealed significant insights into the biomechanical behavior of the implant-bone interface, bone fragments interaction, and stress distribution within the screw.

First, the bone-implant interface analysis demonstrated a non-uniform distribution of contact pressure at the screw threads, primarily concentrated at the upper surface of the threads due to the developed tractive force along the screw axis. Sliding behavior at the interface transitioned from initial sticking to full sliding as rotational acceleration increased, with maximum frictional stresses peaking early and subsequently decreasing due to the transition from static to dynamic friction (**Fig. 3**).

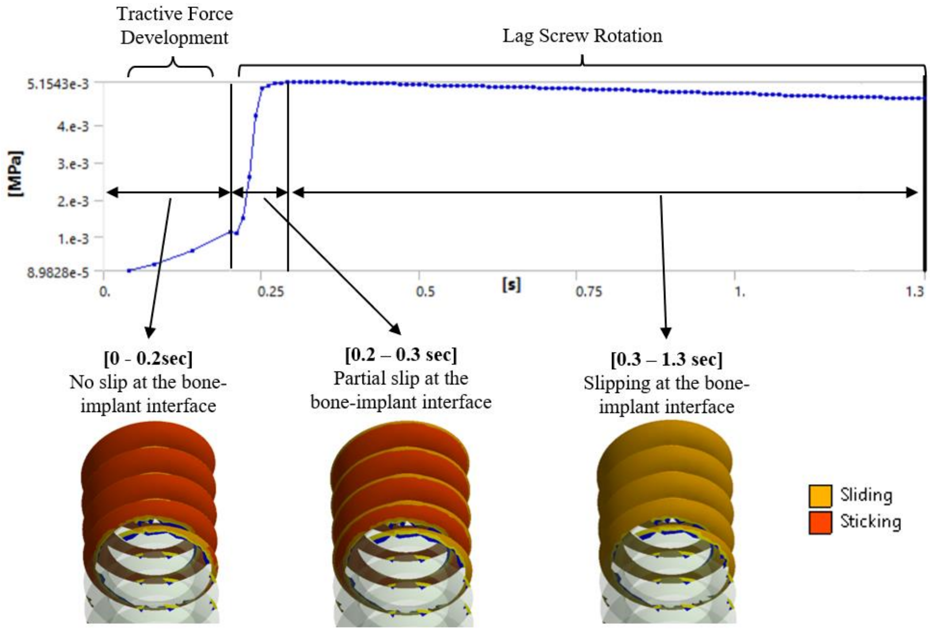

Fig. 3. Contact stress (Top), Contact status (Bottom) at the bone-implant interface

Analysis of the bone fragments interface indicated that relative sliding between the femoral head and shaft was minimal, peaking at 1.55µm. Contact pressure distribution at the fracture interface was non-uniform, with higher pressures developing on the posterior side near the implant hole (**Fig. 4**). Notably, sliding occurred around a rotation center not coincident with the lag screw axis, suggesting geometric sensitivity and highlighting the importance of screw orientation relative to the fracture plane.

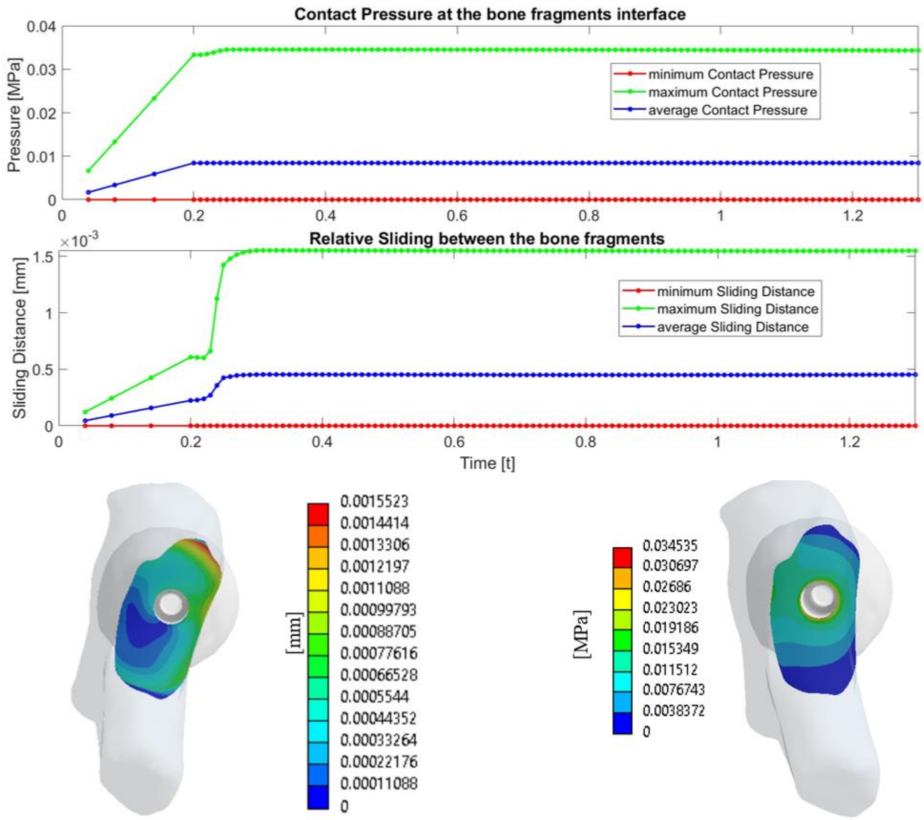

Fig. 4. Time history of contact pressure and relative sliding at the fracture (top), Contour plots of sliding (left) and pressure (right) at t=0.3sec

Stress analysis revealed that the lag screw experienced minimal stress from the applied tractive force, with the maximum von-Mises stress recorded at 1.37 MPa, significantly below the material yield strength (850 MPa) of Ti6Al4V. Stress concentration was observed primarily at the root of the threads due to geometrical transitions in the screw design. Additionally, bending stresses developed due to slight misalignment between the fracture plane and the screw axis were negligible (**Fig. 5**).

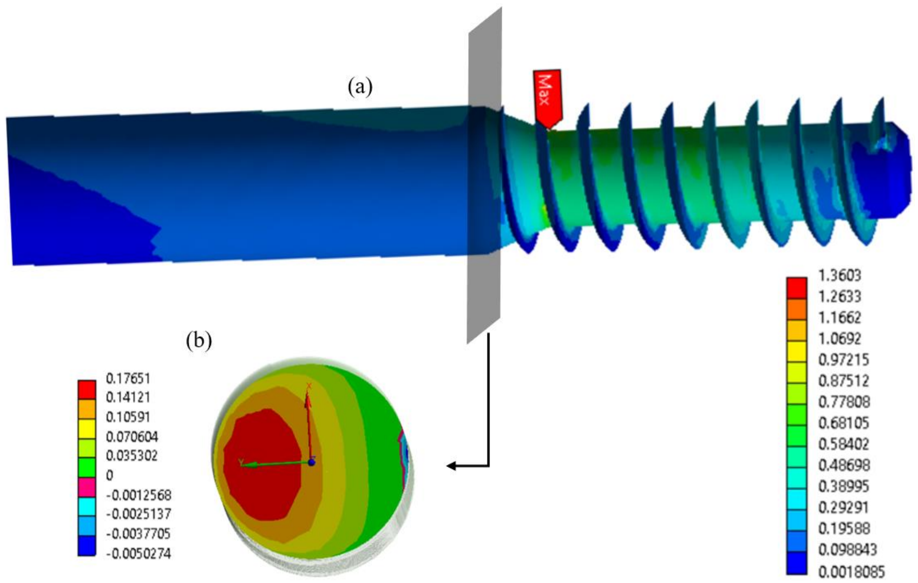

Fig. 5. (a) Von-Mises equivalent stress distribution in the body of the screw and (b) normal stresses on lag screw body section

The equivalent elastic stiffness of the bone-implant assembly varied slightly throughout the procedure, stabilizing around 554474 N/m, confirming the viability of a simplified elastic model for robotic simulation purposes.

The robotic manipulator simulation, aimed at automating lag screw insertion for basicervical femoral neck fracture fixation, yielded promising results. The end-effector successfully maintained the targeted trajectory, with minimal linear displacement along the screw axis during the initial phase of tractive force development (0–0.2 s), corresponding to slight elongation of the compliance spring representing the bone-screw interface stiffness. During the subsequent rotational acceleration phase (0.2–1.2 s), the manipulator accurately followed the angular velocity reference, with negligible positional error (<1%), demonstrating effective position control. The force control scheme exhibited a transient error of up to 7.5% at the initiation of screw rotation, swiftly diminishing and stabilizing within operational requirements (**Fig. 6**). This force overshoot, although brief, underscores the importance of accurate initial force application to minimize femoral head rotation. Despite minor overshoot during transitions, the control system maintained stable and precise force output for the remainder of the procedure.

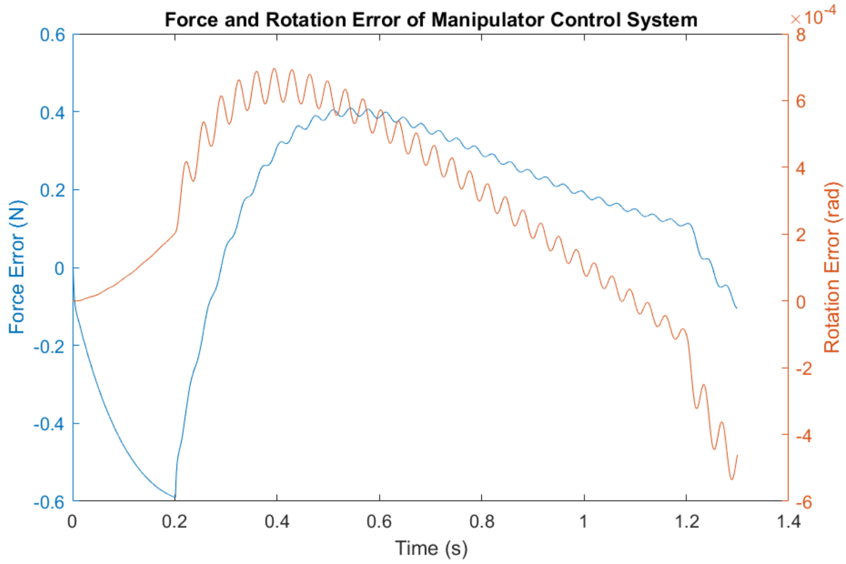

Fig. 6. Rotation and Force errors along the x-axis of the maniuplator end-effector

4 Conclusion

The finite element analysis and robotic simulation presented in this study demonstrate that the empirical surgical technique of applying tractive force along the lag screw's axis prior to rotation successfully minimizes the relative rotational displacement between femoral fragments during the fixation of basicervical femoral neck fractures. The contact behavior at the bone-implant interface, specifically frictional interactions, predominantly governed the sliding response observed between fragments. Notably, the distribution of contact pressures across the fracture interface was uneven, with elevated pressures primarily around the implant and on the posterior side of the fracture, largely due to the non-perpendicular orientation of the lag screw axis relative to the fracture plane. This geometric configuration was found to induce beneficial frictional forces that constrained fragment rotation effectively, though it also introduced slight bending stresses on the lag screw. Despite this bending, peak stress values within the implant remained significantly below the yield strength threshold for Ti6Al4V, indicating a low risk of mechanical failure during insertion.

Simulation results further revealed a complex interplay between the orientation of the lag screw and its effectiveness in maintaining fracture stability. It was demonstrated that adjusting the orientation of screw insertion could optimize interface pressures and reduce undesirable fragment motion. These findings underscore the potential of personalized finite element analyses (FEA) for preoperative planning, suggesting that detailed patient-specific modeling could significantly improve surgical outcomes through tailored screw placement strategies.

Additionally, the robotic manipulator simulation employing a hybrid position/force control scheme in Simulink successfully reproduced the lag screw insertion procedure. The manipulator followed rotational speed reference inputs accurately, with minimal positional errors (less than 1%) and acceptable tractive force control errors (less than 7.5%). These minor deviations, however, occurred predominantly at critical phases of the procedure. The simulation also verified that joint torques remained within operational limits, supporting the practical feasibility of employing a robotic system for semi-automated screw insertion.

Overall, these findings support the potential clinical utility of an integrated robotic system that could automate portions of lag screw insertion, reducing variability and potentially improving patient outcomes. The study underscores the potential of patient-specific finite element modelling and robotic automation in enhancing the precision and reliability of orthopedic surgical interventions.

References

1. Veronese, N., Maggi, S.: Epidemiology and social costs of hip fracture. Injury. 49, 1458–1460 (2018). https://doi.org/10.1016/j.injury.2018.04.015.
2. Kanis, J.A., Odén, A., McCloskey, E. V., Johansson, H., Wahl, D.A., Cooper, C.: A systematic review of hip fracture incidence and probability of fracture worldwide, (2012). https://doi.org/10.1007/s00198-012-1964-3.
3. Cooper, C., Cole, Z.A., Holroyd, C.R., Earl, S.C., Harvey, N.C., Dennison, E.M., Melton, L.J., Cummings, S.R., Kanis, J.A.: Secular trends in the incidence of hip and other osteoporotic fractures. Osteoporosis International. 22, 1277–1288 (2011). https://doi.org/10.1007/s00198-011-1601-6.
4. Ferris, H., Brent, L., Sorensen, J.: Cost of hospitalisation for hip fracture—findings from the Irish hip fracture database. Osteoporosis International. 33, 1057–1065 (2022). https://doi.org/10.1007/s00198-021-06294-7.
5. Dekhne, M.S., Thomas, H.M., Haider, T., Mortensen, S., Rodriguez, E.K., Weaver, M.J., von Keudell, A.: Treatment and outcomes of basicervical femoral neck fractures: A systematic review. Journal of Orthopaedic Surgery. 29, (2021). https://doi.org/10.1177/23094990211003344.
6. Kijima, H., Yamada, S., Kawano, T., Komatsu, M., Iwamoto, Y., Konishi, N., Kubota, H., Tazawa, H., Tani, T., Suzuki, N., Kamo, K., Sasaki, K., Fujii, M., Nagahata, I., Miura, T., Igarashi, S., Miyakoshi, N.: Characteristics and Treatment Strategies for Basicervical and Transcervical Shear Fractures of the Femoral Neck. J Clin Med. 12, (2023). https://doi.org/10.3390/jcm12227024.
7. Lee, Y.K., Yoon, B.H., Hwang, J.S., Cha, Y.H., Kim, K.C., Koo, K.H.: Risk factors of fixation failure in basicervical femoral neck fracture: Which device is optimal for fixation? Injury. 49, 691–696 (2018). https://doi.org/10.1016/j.injury.2018.02.009.

8. Yoo, J. Il, Cha, Y., Kwak, J., Kim, H.Y., Choy, W.S.: Review on Basicervical Femoral Neck Fracture: Definition, Treatments, and Failures. Hip Pelvis. 32, 170–181 (2020). https://doi.org/10.5371/hp.2020.32.4.170.
9. Sundkvist, J., Brüggeman, A., Sayed-Noor, A., Möller, M., Wolf, O., Mukka, S.: Epidemiology, classification, treatment, and mortality of adult femoral neck and basicervical fractures: an observational study of 40,049 fractures from the Swedish Fracture Register. J Orthop Surg Res. 16, (2021). https://doi.org/10.1186/s13018-021-02701-1.
10. Massoud, E.I.E.: Fixation of basicervical and related fractures. Int Orthop. 34, 577–582 (2010). https://doi.org/10.1007/s00264-009-0814-1.
11. Murakami, S., Zhao, Y., Mizuno, K., Yamada, M., Yokoyama, Y., Yamada, Y., Jinzaki, M.: Finite element analysis of hip fracture risk in elderly female: The effects of soft tissue shape, fall direction, and interventions. J Biomech. 172, 112199 (2024). https://doi.org/10.1016/j.jbiomech.2024.112199.
12. Fleps, I., Pálsson, H., Baker, A., Enns-Bray, W., Bahaloo, H., Danner, M., Singh, N.B., Taylor, W.R., Sigurdsson, S., Gudnason, V., Ferguson, S.J., Helgason, B.: Finite element derived femoral strength is a better predictor of hip fracture risk than aBMD in the AGES Reykjavik study cohort. Bone. 154, 116219 (2022). https://doi.org/10.1016/j.bone.2021.116219.
13. Cao, X., Keyak, J.H., Sigurdsson, S., Zhao, C., Zhou, W., Liu, A., Lang, T.F., Deng, H.-W., Gudnason, V., Sha, Q.: A new hip fracture risk index derived from FEA-computed proximal femur fracture loads and energies-to-failure. Osteoporosis International. 35, 785–794 (2024). https://doi.org/10.1007/s00198-024-07015-6.
14. Huang, Q., Zhang, C., Bai, H., Wang, Q., Li, Z., Lu, Y., Ma, T.: Biomechanical evaluation of two modified intramedullary fixation system for treating unstable femoral neck fractures: A finite element analysis. Front Bioeng Biotechnol. 11, (2023). https://doi.org/10.3389/fbioe.2023.1116976.
15. Özer, A., Öner, K., Emin Okutan, A., Salih Ayas, M.: Comparative finite element analysis of four different internal fixation implants for Pauwels type III femoral neck fractures in various fracture angles in the sagittal plane. Jt Dis Relat Surg. 33, 352–358 (2022). https://doi.org/10.52312/jdrs.2022.676.
16. Eberle, S., Gerber, C., von Oldenburg, G., Högel, F., Augat, P.: A Biomechanical Evaluation of Orthopaedic Implants for Hip Fractures by Finite Element Analysis and In-Vitro Tests. Proc Inst Mech Eng H. 224, 1141–1152 (2010). https://doi.org/10.1243/09544119JEIM799.
17. Yang, P., Lin, T.-Y., Xu, J.-L., Zeng, H.-Y., Chen, D., Xiong, B.-L., Pang, F.-X., Chen, Z.-Q., He, W., Wei, Q.-S., Zhang, Q.-W.: Finite element modeling of proximal femur with quantifiable weight-bearing area in standing position. J Orthop Surg Res. 15, 384 (2020). https://doi.org/10.1186/s13018-020-01927-9.
18. Ding, K., Zhu, Y., Zhang, Y., Li, Y., Wang, H., Li, J., Chen, W., Zhang, Q., Zhang, Y.: Proximal femoral bionic nail—a novel internal fixation system for the treatment of femoral neck fractures: a finite element analysis. Front Bioeng Biotechnol. 11, (2023). https://doi.org/10.3389/fbioe.2023.1297507.

19. Kim, C.-J., Lee, J.S., Goh, T.S., Shin, W.C., Lee, C.: Finite element analysis of fixation stability according to reduction position for internal fixation of intertrochanteric fractures. Sci Rep. 14, 19214 (2024). https://doi.org/10.1038/s41598-024-69783-9.
20. Rhyu, K.H., Kim, Y.H., Park, W.M., Kim, K., Cho, T.-J., Choi, I.H.: Application of finite element analysis in pre-operative planning for deformity correction of abnormal hip joints – a case series. Proc Inst Mech Eng H. 225, 929–936 (2011). https://doi.org/10.1177/0954411911407247.
21. He, Y., Liu, Y., Yin, B., Wang, D., Wang, H., Yao, P., Zhou, J.: Application of Finite Element Analysis Combined With Virtual Computer in Preoperative Planning of Distal Femoral Fracture. Front Surg. 9, (2022). https://doi.org/10.3389/fsurg.2022.803541.
22. Wu, X., Wang, Y., Zhu, G., Wang, J., Tian, W.: An Overview of Robotic Applications in Traumatic Orthopedics. In: Navigation Assisted Robotics in Spine and Trauma Surgery. pp. 153–158. Springer Singapore, Singapore (2020). https://doi.org/10.1007/978-981-15-1846-1_19.
23. Kalavrytinos, D., Koutserimpas, C., Kalavrytinos, I., Dretakis, K.: Expanding Robotic Arm-Assisted Knee Surgery: The First Attempt to Use the System for Knee Revision Arthroplasty. Case Rep Orthop. 2020, 1–5 (2020). https://doi.org/10.1155/2020/4806987.
24. Fan, X., Wang, Y., Zhang, S., Xing, Y., Li, J., Ma, X., Ma, J.: Orthopedic surgical robotic systems in knee arthroplasty: a comprehensive review. Front Bioeng Biotechnol. 13, (2025). https://doi.org/10.3389/fbioe.2025.1523631.
25. Diaz-Aguilar, L.D., Brown, N.J., Bui, N., Alvandi, B., Pennington, Z., Gendreau, J., Jeswani, S.P., Pham, M.H., Santiago-Dieppa, D.R., Nguyen, A.D.: The use of robot-assisted surgery for the unstable traumatic spine: A retrospective cohort study. North American Spine Society Journal (NASSJ). 15, 100234 (2023). https://doi.org/10.1016/j.xnsj.2023.100234.
26. Ferraguti, F., Farsoni, S., Bonfè, M.: Augmented Reality and Robotic Systems for Assistance in Percutaneous Nephrolithotomy Procedures: Recent Advances and Future Perspectives. Electronics (Basel). 11, 2984 (2022). https://doi.org/10.3390/electronics11192984.
27. Fedorov, A., Beichel, R., Kalpathy-Cramer, J., Finet, J., Fillion-Robin, J.-C., Pujol, S., Bauer, C., Jennings, D., Fennessy, F., Sonka, M., Buatti, J., Aylward, S., Miller, J. V., Pieper, S., Kikinis, R.: 3D Slicer as an image computing platform for the Quantitative Imaging Network. Magn Reson Imaging. 30, 1323–1341 (2012). https://doi.org/10.1016/j.mri.2012.05.001.
28. Taddei, F., Schileo, E., Helgason, B., Cristofolini, L., Viceconti, M.: The material mapping strategy influences the accuracy of CT-based finite element models of bones: An evaluation against experimental measurements. Med Eng Phys. 29, 973–979 (2007). https://doi.org/10.1016/j.medengphy.2006.10.014.
29. Schileo, E., Dall'Ara, E., Taddei, F., Malandrino, A., Schotkamp, T., Baleani, M., Viceconti, M.: An accurate estimation of bone density improves the accuracy of subject-specific finite element models. J Biomech. 41, 2483–2491 (2008). https://doi.org/10.1016/j.jbiomech.2008.05.017.

30. Morgan, E.F., Bayraktar, H.H., Keaveny, T.M.: Trabecular bone modulus–density relationships depend on anatomic site. J Biomech. 36, 897–904 (2003). https://doi.org/10.1016/S0021-9290(03)00071-X.
31. Grant, J.A., Bishop, N.E., Götzen, N., Sprecher, C., Honl, M., Morlock, M.M.: Artificial composite bone as a model of human trabecular bone: The implant–bone interface. J Biomech. 40, 1158–1164 (2007). https://doi.org/10.1016/j.jbiomech.2006.04.007.